

RESEARCH

Open Access



Mechanical Properties of Ultra-High Performance Concrete (UHPC) and Ultra-High Performance Fiber-Reinforced Concrete (UHPFRC) with Recycled Sand

Donguk Choi¹, Kyungchan Hong^{2*} , Munkhtuvshin Ochirbud¹, Didar Meiramov² and Piti Sukontaskul³

Abstract

Use of high-cost raw materials such as quartz sand can limit wider application of ultra-high performance concrete in concrete construction. In this experimental study, recycled sand was used to fabricate ultra-high performance concrete (UHPC) and ultra-high performance fiber-reinforced concrete (UHPFRC). Green UHPC with ordinary Portland cement and industrial by-products such as silica fume, fly ash, as well as recycled sand was first developed through two-step packing density tests to optimize the mix design. UHPFRC was then developed based on the UHPC mix designs and by using 1%, 2%, or 3% 13-mm straight steel fibers (SSF). The compressive strength, elastic modulus, and flexural tensile strength was 128 MPa, 46.9 GPa, and 11.9 MPa, respectively, after 28 days at water-to-binder ratio of 0.17 and with 2% SSFs. All high-performance concretes in this work utilized 100% commercially available recycled sand that was produced by wet processing method. Mechanical characteristics such as strength, elastic modulus, and density, absorption, and voids of the UHPC/UHPFRC were investigated. Development of autogenous shrinkage of UHPC/UHPFRC with recycled sand was monitored for 12 weeks, while mercury intrusion porosimetry test and scanning electron microscopy were performed for microstructural investigation. Finally, the environmental impacts and economical aspects of the green UHPC were evaluated by life cycle assessment (LCA) and cost analysis.

Keywords UHPC, UHPFRC, Recycled sand, Experimental packing density, Environmental impact

1 Introduction

As a result of active research during the past decades, recycled aggregates produced from waste concrete can be used nowadays to partly replace natural aggregates

despite certain characteristics of RAs including low density and high water absorption (Chinzorigt et al., 2020; Silva et al., 2014): e.g., EN 206 (2021) prescribes the minimum requirements for the mechanical properties of the recycled coarse aggregates and the method of use. While the use of recycled fine aggregates for concrete is still limited, both recycled coarse aggregates and recycled fine aggregates are often used to produce concrete in some countries including South Korea, China, Japan as well as some European countries such as The Netherlands (KS F 2573, 2014, Brito et al., 2013).

Ultra-high performance concrete (UHPC) is an advanced cementitious composite with very high strength, good workability, and excellent durability (Amran et al., 2022; Bahmani & Mostofinejad, 2022; Du

Journal information: ISSN 1976-0485 / eISSN 2234-1315.

*Correspondence:

Kyungchan Hong
ghdrudcks96@hknu.ac.kr

¹ Hankyong National University Industry Academic Cooperation Foundation, Anseong, Republic of Korea

² Department of Architectural Engineering, Hankyong National University, Anseong, Republic of Korea

³ Department of Civil Engineering, King Mongkut's University of Technology North Bangkok, Bangkok, Thailand

et al., 2021; Ravichandran et al., 2022; Yang et al., 2022; Yu et al., 2023). Because the maximum packing of the concrete ingredients will result in low-porosity concrete with very high strength, the methods to obtain possible packing of concrete are needed (Sohail et al., 2018). To this end, several packing models have been developed (Stovall & Larrard, 1986; Larrard & Sedran, 1994, 2002; Richard & Cheyrezy, 1995).

High amount of cement, silica fume, fine quartz sand, quartz powder to produce UHPC raises their cost and carbon footprint (Jaramillo-Murcia et al., 2022). In an attempt to fabricate green UHPCs with reduced environmental footprint, researchers used diverse recycled materials such as fly ash (Ahmed et al., 2021), blast furnace slag and rice husk ash (Ha et al., 2022), recycled powder (Mao et al., 2019), crushed glass/recycled glass powder (Dawood & Abdullah, 2021; Jaramillo-Murcia et al., 2022; Luo et al., 2022; Soliman & Tagnit-Hamou, 2017) as well as recycled aggregates (Jiang et al., 2019; Leng et al., 2023; Salahuddin et al., 2020; Zhang et al., 2018; Zhou et al., 2021). In a study by Zhang et al. (2018), recycled fine aggregates were used to fabricate UHPC while the recycled fine aggregates replaced natural river sand by 0%, 25%, 50%, 75%, 100%. Ordinary Portland cement, silica fume, and quartz powder were used as solid constituents and, in addition, straight steel fibers were used while the water-to-binder ratio was 0.14. Mixtures were cured under two different curing conditions: standard cure and autoclaving. They have observed that the recycled fine aggregate replacement ratio affected the mechanical properties of UHPC mainly by introducing more interfacial transition zones (ITZs) and more old cement matrix (adhered mortar). As a result, the hardness of ITZ decreased and the thickness of ITZ increased. Autoclaving could improve the quality of ITZ by reducing their thickness and enhancing their microhardness. Salahuddin et al. (2020) reported that 108 MPa RPC was successfully fabricated using up to 50% replacement of natural sand with recycled sand, but the strength degraded at 75% replacement. Leng et al. (2023) used natural coarse aggregate (NCA), recycled coarse aggregate (RCA), and carbonated recycled coarse aggregate (CRCA) to fabricate UHPC which utilized natural sand. They reported that 28d compressive strength increased from 112 MPa, 117 MPa, to 123 MPa in the order of NA, RCA, CRCA concrete. Autogenous shrinkage of RCA was largest, followed by NA, and CRCA concrete.

In general, it has been generally accepted among researchers that the maximum amount of the recycled fine aggregates replacing the natural fine aggregates is about 30–60% in normal- to high-strength concretes considering the reduction in strength and elastic modulus, increased shrinkage and creep, and durability aspects

of the recycled aggregate concrete (Chinzorigt et al., 2020; Jiang et al., 2019; Salahuddin et al., 2020; Zhang et al., 2022). Up to 50% replacement of recycled sand was used to fabricate UHPC (Salahuddin et al., 2020). There is a clear need to use more actively utilized recycled sand to replace costly and dwindling natural resources (quartz sand or natural silica sand). Recently, Naidanjav et al. (2022) utilized ordinary Portland cement, silica fume, waste glass powder, and fly ash as binder materials and reported fabrication of 100-MPa RPC with wet-processed 100% recycled sand, while water-to-binder ratio was 0.18. Current work is a continuation of the work by Naidanjav et al. in the same laboratory to fabricate low-binder UHPC with commercial wet-processed high-quality recycled sand (see Fig. 2). Main motivation was to produce the UHPC with complete replacement of quartz sand/silica sand by recycled sand together with reduced Portland cement content to produce green UHPC with reduced environmental footprint.

2 Material Properties and Preparation for Test

2.1 Cement, Substitutive Cementitious Materials and Filler

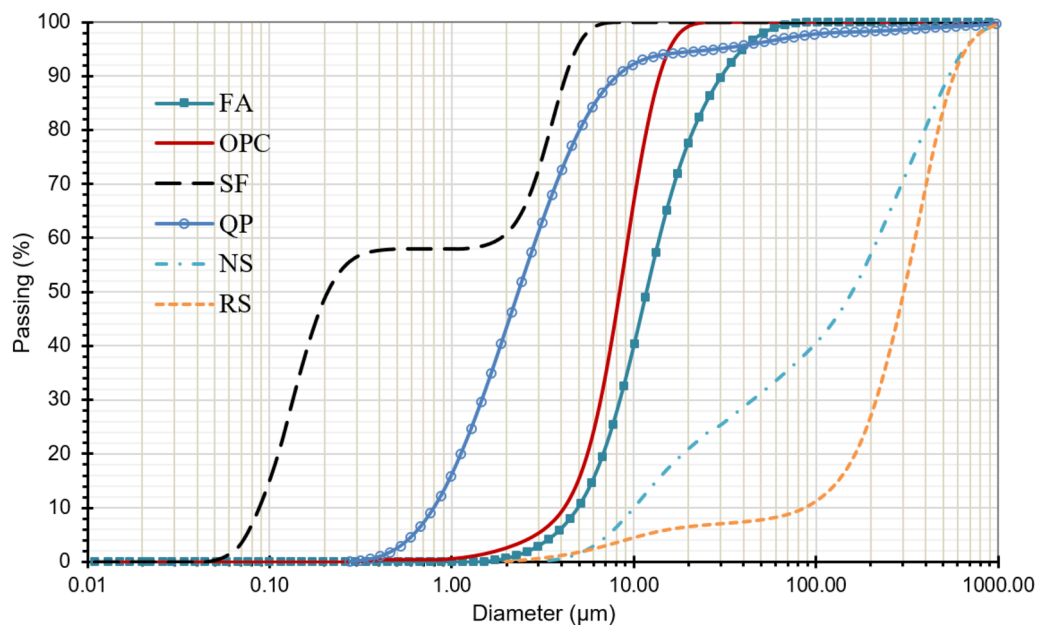
Type-1 Portland cement (OPC, 42.5 MPa grade) was used as the main binder material. A commercial grade silica fume (SF) with specific gravity of 2.22, d_{50} of 0.24 μm , and silica content of 93% was utilized while Type-F fly ash (FA) was the byproduct of a coal-burning power plant with specific gravity of 2.50 and d_{50} of 7.0 μm . Quartz powder (QP) with specific gravity of 2.65, d_{50} of 2.4 μm , and SiO_2 content of 98% was used as the filler material. Table 1 summarizes the chemical composition of cement, substitutive cementitious materials (SCM), filler as well as fine aggregates determined by X-ray fluorescence. Fig. 1 shows the gradation of all constituents determined by laser diffraction analysis.

2.2 Fine Aggregates

Two different fine aggregates, natural crushed sand (NS) and recycled sand (RS), were employed. NS was used to develop a reference mix. Waste concrete was the source material of the commercial recycled sand produced through wet processing technology as shown in Fig. 2, which schematically illustrates the wet processing procedure used to produce high-quality recycled sand in South Korea. Fig. 3 shows SEM images of RS and NS, where both RS and NS have angular morphology while the surface of RS is rough due to adhered small grains and loose particles in comparison to the relatively smooth surface of NS. Table 2 summarizes the physical properties of the fine aggregates in terms of bulk specific gravity (BSG), unit weight (UW), water absorption (WA), fineness modulus (FM), void ratio, and % passing 0.08-mm sieve. As shown in Table 2,

Table 1 Chemical composition of binders, filler and fine aggregates

Component	OPC	SF	FA	QP	RS	NS
CaO	66.1	0.95	2.53	0.27	21.2	2.06
SiO ₂	19.0	92.6	66.2	97.9	54.7	71.4
Al ₂ O ₃	4.83	0.36	20.4	0.51	11.0	12.7
SO ₃	2.17	0.81	–	–	0.91	0.17
Fe ₂ O ₃	3.68	0.96	4.72	0.05	4.27	4.39
MgO	2.19	1.03	0.99	–	1.75	2.16
K ₂ O	1.07	2.16	0.73	0.01	3.17	4.18
TiO ₂	0.26	–	0.94	0.13	0.46	0.57
Na ₂ O	0.11	0.64	0.37	–	1.91	1.91
P ₂ O ₅	0.14	0.15	0.64	1.06	0.15	0.15

**Fig. 1** Gradation of OPC, SCMs, filler and fine aggregates

BSG is lower and WA is higher for RS than the corresponding values of NS due to the presence of adhered mortar (or adhered paste) originated from mother concrete and attached to surface of the natural fine aggregates in RS.

2.3 Fibers

Brass-coated straight steel fibers (SSFs) were used to fabricate UHPFRC. The brass coating protects the steel fibers from corrosion, improves tensile performance, and reduces friction among fibers thus can prevent fiber balling. Length, diameter, and specific gravity of SSF are 13 mm, 0.3 mm, and 7.8, respectively.

2.4 Chemical Admixtures

Polycarboxylate superplasticizer (SP) with solid content of 35% was used for all mixtures. Small amount of defoaming agent (DF) was also utilized in an attempt to fabricate UHPC and UHPFRC with the minimum air voids.

2.5 Mixing

For the UHPC mixtures, all powder materials (OPC, SCMs, and filler) except sand were first mixed at low speed (100 rpm) for 4 m using a planetary mixer. Then about 90% water with SP and DF was added and the mixture was mixed for 4 m (2 m at 100 rpm and 2 m at

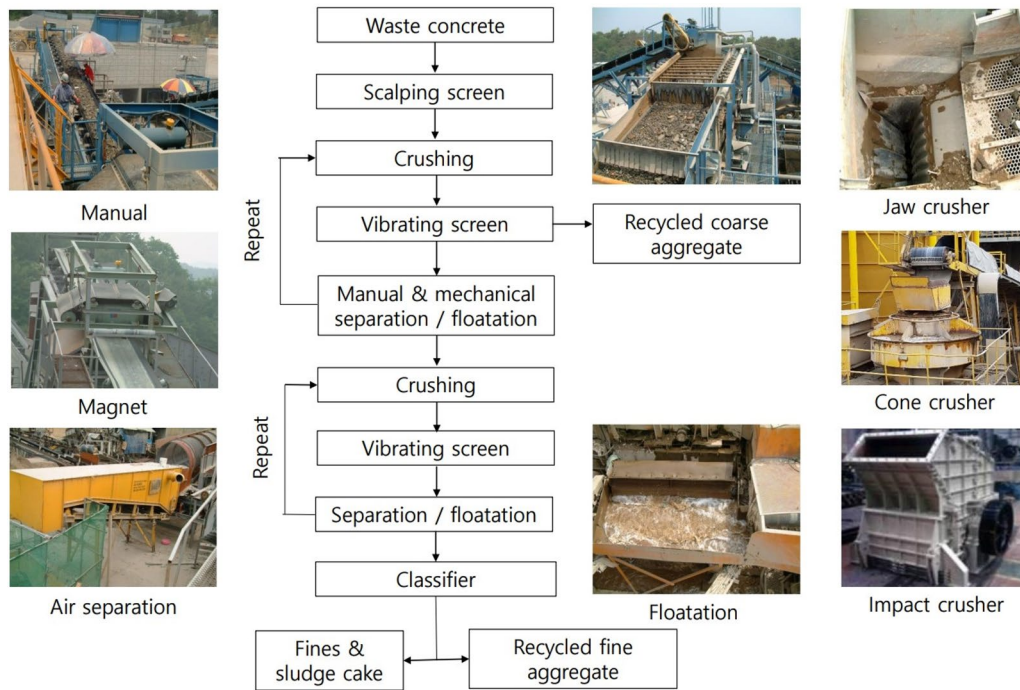


Fig. 2 Production process of recycled aggregates (wet process)

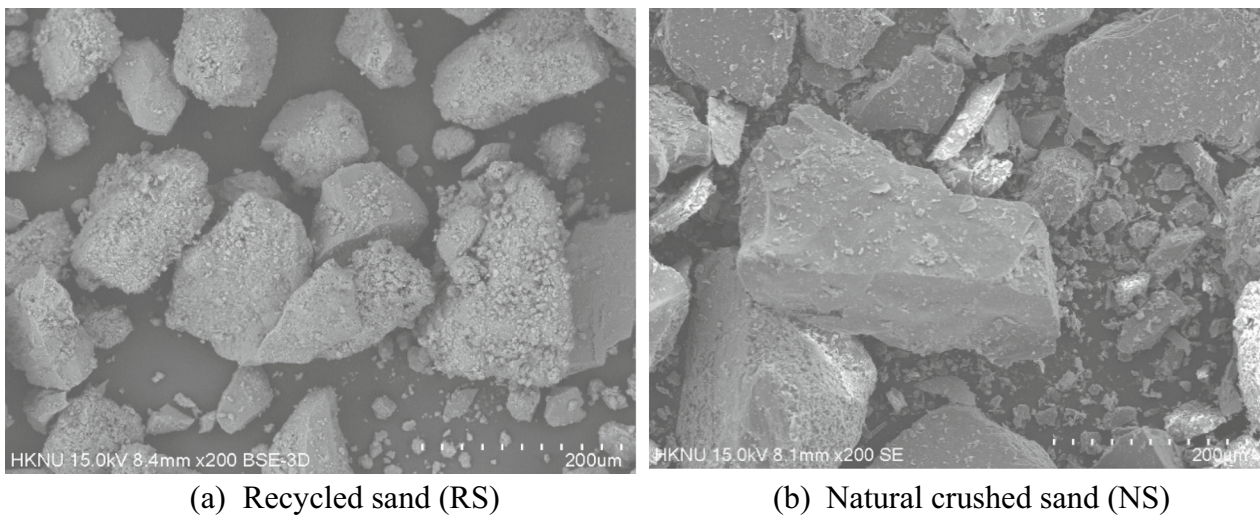


Fig. 3 SEM image of fine aggregates

Table 2 Mechanical properties of fine aggregates

Type	BSG _{SSD}	BSG _{OD}	UW (kg/m ³)	WA (%)	FM	Void ratio (%)	% passing 0.08-mm sieve
NS	2.66	2.64	1709	0.93	3.09	35.3	2.65
RS	2.46	2.34	1471	5.12	3.19	37.1	1.48

180 rpm). Sand prepared in surface saturated dry (SSD) condition and remaining 10% water were added, and mixed at high speed for 4 m. Then the mixture was finally mixed for additional 4 m. The mixing sequence was basically the same for the UHPFRC mixes while the difference was the manual feeding of the short fibers at the low mixing speed to evenly disperse fibers prior to the final mixing.

2.6 Casting and Method of Cure

50 mm × 50 mm × 50 mm cube specimens were made for the compressive strength test 7 days and 28 days after casting while 40 mm × 40 mm × 160 mm prisms were used for the flexural test by 3-point loading 28 days after casting. In addition, Φ 100 mm × 200 mm cylindrical specimens were used to determine the elastic modulus following ASTM C469-02 (2022) procedure and monitor the stress–strain behavior of UHPC and UHPFRC under uniaxial compression. All specimens were covered by double 0.1-mm-thick polyethylene sheets to prevent

moisture loss right after casting for 1 day, demolded after 24 h, and cured under water (18–23 °C) until testing.

The compressive test for cubes and cylinders as well as the flexural test of prisms were performed under displacement control using Instron 4495 universal testing machine (UTM) with capacity of 1200 kN at crosshead speed of 0.5 mm/m. In addition, the prisms were tested following ASTM C642 (2013) procedure to determine, void, water absorption, and density after 28 days.

2.7 Autogenous Shrinkage

The autogenous shrinkage of three different UHPC mixes was monitored for 12 weeks after casting: two mixes with RS and one mix with NS. The test setup and the test method in general followed KS F 2586 (2021). Fig. 4 shows the test setup with 100 mm × 100 mm × 400 mm steel mold. Teflon tape was applied on top of 5-mm-thick acrylic plate assembly placed on the horizontal surface, which was folded into the box-like shape, and placed inside the steel mold. 0.1-mm-thick polyethylene film (PE, double layers) was then loosely placed inside the acrylic box with the Teflon tape which eliminated

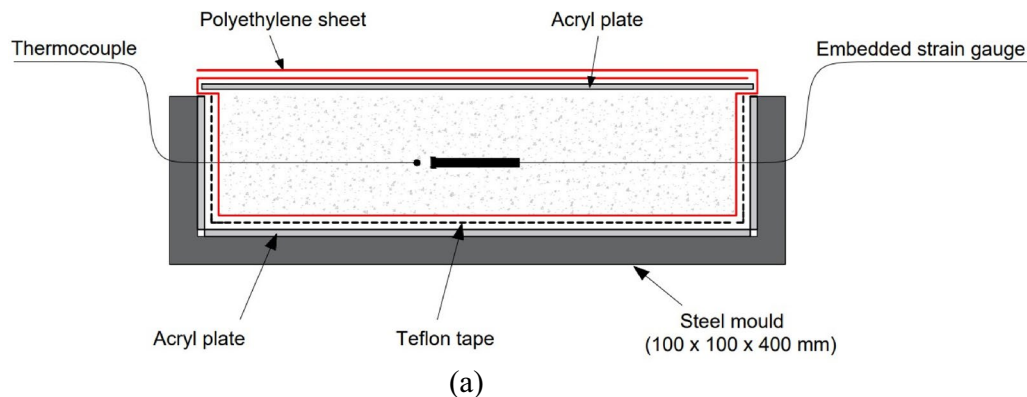


Fig. 4 Autogenous shrinkage test setup: Modified from KS F 2586: 2021. (a) Cross-section of a shrinkage test specimen. (b) Autogenous shrinkage test and measurement under progress Additional name for Fig. 4

friction. The acrylic box was topped with a cover plate, while the PE film completely covered the concrete to avoid moisture loss as shown in Fig. 4. An embedded type 50-mm electronic strain gauge and a thermocouple were installed at center before casting the fresh mixture. All specimens were placed in an environmental chamber ($T=20\text{ }^{\circ}\text{C}$, $\text{R.H.}=60\%$), while the shrinkage evolution was continuously recorded using a data logger. Two replicate specimens were tested.

3 Packing Density Test

In this study, an existing experimental packing density methodology (Kwan & Fung, 2009) was employed as the effect of water which lubricates the solid particles is included in this experimental approach while the theoretical models deal with the solid particles only (Larrad & Sedran, 1994; Funk & Dinger, 1994). The experimental method was applied in two steps: (1) dry packing density test and (2) wet packing density test. A mixture of dry constituents with the minimum void ratio was first determined by the dry packing density test where all constituents except SF, QP, and water were used. The wet packing density test was performed based on the results of the dry packing density test, and used all constituents including water. Mass of each constituent was determined that resulted in the maximum packing (maximum solid ratio). A cylindrical container was used. Mixed dry constituents or wet mixtures were poured into the container to about one-third of the container height while this procedure was repeated three times. Each layer was loosely placed,

compacted 25 times by a tamping rod, or vibrated for 15 s on the vibrating table. Mass of the container with the dry constituents/wet mixture was measured and the solid ratio was determined.

3.1 Dry Packing Density Test with Recycled Sand

The binders consisted of OPC, SF, FA as well as QP which was used as the filler material. The absolute volume-base mix design proceeded as follows. The amount of FA, which was used to improve flow of the mixtures due to its perfect spherical morphology, was prefixed to replace binders by 10% (by vol.). Then, four different binder-to-sand ratios were tested in the dry packing density test (45%:55%, 50%:50%, 55%:45%, 60%:40% by vol.), where 100% RS with the maximum particle size of 1.2 mm was used as shown in Table 3 which also shows the ideal state for the dry mixtures with zero void (Theoretical wt.). Three different dry densities were measured: Loose density (Loose), rodded density (Rodded), and density after vibration (Vibrated). The solid ratio and the void ratio were determined using Eqs. (1) and (2):

$$\text{Solidratio} = \frac{\text{Measuredwt.}}{\text{Theoreticalwt.}} \quad (1)$$

$$\text{Voidratio} = 1 - \text{solidratio} \quad (2)$$

Table 4 and Fig. 5a show the results of the dry packing density test. As shown in Table 4, the void ratio varies depending on the method of compaction and becomes smaller in the order of loose > rodded > vibrated while

Table 3 Mix proportion for dry packing density test with recycled sand

Index	Volume-base (unit: m^3)				Mass-base (unit: kg/m^3)			
	OPC	FA	RS	Total	OPC	FA	RS	Theoretical wt
D-RS-1	0.405	0.045	0.550	1.00	1276	113	1353	2741
D-RS-2	0.450	0.050	0.500	1.00	1418	125	1230	2773
D-RS-3	0.495	0.055	0.450	1.00	1559	138	1107	2804
D-RS-4	0.540	0.060	0.400	1.00	1701	150	984	2835

D-RS-n, D dry packing, RS recycled sand, n batch number

Table 4 Results of dry packing density test with recycled sand

Index	Solid ratio			Void ratio		
	Loose	Rodded	Vibrated	Loose	Rodded	Vibrated
D-RS-1	0.487	0.574	0.611	0.513	0.426	0.389
D-RS-2	0.470	0.557	0.584	0.530	0.443	0.416
D-RS-3	0.456	0.539	0.565	0.544	0.462	0.436
D-RS-4	0.441	0.522	0.546	0.559	0.479	0.454

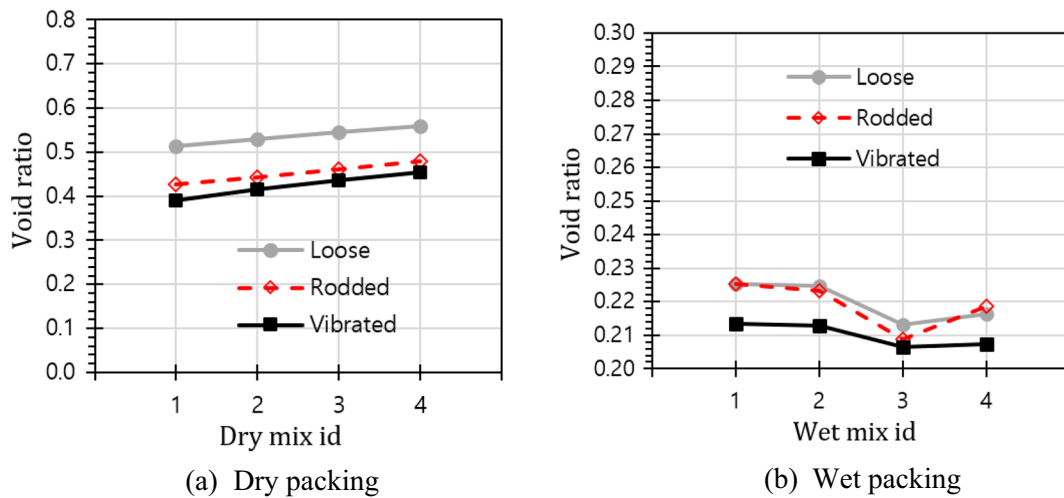


Fig. 5 Results of packing density tests with recycled sand

the void ratio is 0.389, 0.416, 0.436, and 0.454, respectively, for D-RS-1, -2, -3, and -4 after vibration. The similar trend is shown under loose and rodded conditions in Table 4 and Fig. 5a. The dry packing density test results show that the void ratio is the smallest (38.9%) when the binder-to-sand ratio is 45%:55% by vol. for D-RS-1. It is noted that, the void ratio increases with increasing binder-to-sand ratio with the solid constituents used in this study while the volumetric ratio of 45%:55% is converted to the mass ratio (B/S) of 0.49 in Table 3. The current test results indicate that the packing is efficient when the B/S is less than 0.5 (for selected combination of constituents), which suggests a possibility of using smaller amount of binder to fabricate UHPCs with reduced environmental impact.

3.2 Wet Packing Density Test with Recycled Sand

Water, SF, and QP were used in addition to OPC, FA, and RS for the wet packing density test. Binder-to-sand ratio was 45%:55% by vol. as a result of the dry packing density test. The total amount of QP and SF that replaced the binder was prefixed at 20% of binder by vol. while the ratio of SF:QP varied: 20%:0%, 15%:5%, 10%:10%, 5%:15% by vol. Water-to-binder ratio (W/B) was 0.20. Table 5 shows the mix design of the wet packing density test. For the wet packing density test, the solid ratio can be calculated by Eq. (3):

$$\text{Solid ratio} = 1 - \text{entrapped air} - \text{water}. \quad (3)$$

In the ideal status (i.e., zero void), all space is filled by binder, sand, and water such that Eqs. (4) and (5) hold:

$$\text{Theoretical wt.} = \text{solid wt.} + \text{water wt.} \quad (4)$$

$$\text{Measured vol. without air} = \frac{\text{Measured wt.}}{\text{Theoretical wt.}}. \quad (5)$$

Table 6 and Fig. 5b show the results of the wet packing density test. As shown in Table 6 and Fig. 5b, the void ratio becomes smaller in the order of loose > rodded > vibrated, where W-RS-3 has the smallest void ratio of 0.213, 0.209, and 0.207 (solid ratio = 0.787, 0.791, and 0.793) under loose, rodded, and vibrated conditions, respectively. Therefore, the mix design of W-RS-3 with a solid ratio of 79.3% after vibration was chosen as an optimum mix.

3.3 Dry and Wet Packing Density Test Results with Natural Sand

The mixture design of the reference mix with NS was carried out using the same experimental methodology as described in Clauses 3.1 and 3.2, while NS was used instead of RS. Aside from different type of sand, the other difference was the ternary system of the reference mix where OPC, SF, and QP were used instead of the four-component system of OPC, SF, FA, and QP used for the UHPC with RS. The adoption of the ternary system excluding FA was based on preliminary study where the mixture with NS showed better flowability than the mixture with RS as the adhered mortar in RS absorbs water and reduces the workability. Water-to-binder ratio was kept the same (W/B = 0.20) and the same amount of the chemical admixtures was applied for the reference mix with NS as that used for the mixes with RS. Table 7 summarizes the optimized mix design of the reference mix determined by the two-step packing density tests. In Table 7, the solid ratio of the reference mixture (W-NS-1)

Table 5 Mix proportion for wet packing density test with recycled sand

Index	Volume-base (m ³)						
	OPC	FA	SF	QP	RS	W	Total
W-RS-1	0.260	0.029	0.072	0.000	0.442	0.196	1.0
W-RS-2	0.260	0.029	0.054	0.018	0.441	0.197	1.0
W-RS-3	0.260	0.029	0.036	0.036	0.441	0.199	1.0
W-RS-4	0.259	0.029	0.018	0.054	0.440	0.200	1.0
Index	Mass-base (kg/m ³)						
	OPC	FA	SF	QP	RS	W	Theoretical wt
W-RS-1	820	72	161	0	1088	196	2337
W-RS-2	819	72	120	48	1086	197	2343
W-RS-3	818	72	80	96	1084	199	2348
W-RS-4	817	72	40	143	1082	200	2354

1. W-RS-*n*, *W* wet packing, *RS* recycled sand, *n* batch number; 2. binder:sand = 45%:55% by vol.; 3. FA replaces OPC by 10% by vol.; 4. (SF + QP) replaces binder by 20% by vol.; 5. SF:QP = 20%:0%, 15%:5%, 10%:10%, 5%:15%; 6. W/B = 0.20; 7. SP and DF amount is 4.0% and 0.1% of total binder amount, respectively, in all mixes

Table 6 Results of wet packing density test with recycled sand

Index	Solid ratio			Void ratio		
	Loose	Rodded	Vibrated	Loose	Rodded	Vibrated
W-RS-1	0.7748	0.7747	0.7866	0.2252	0.2253	0.2134
W-RS-2	0.7753	0.7767	0.7871	0.2247	0.2233	0.2129
W-RS-3	0.7868	0.7912	0.7934	0.2132	0.2088	0.2066
W-RS-4	0.7836	0.7815	0.7926	0.2164	0.2185	0.2074

Table 7 Results of experimental packing density tests for mix with natural sand

	Volume-base (m ³)					Void ratio (solid ratio)	
	C	SF	QP	NS	W	Total	
W-NS-1 (Reference)	0.283	0.018	0.053	0.432	0.214	1.0	0.215 (0.785)
	Mass-base (kg/m ³)						
	C	SF	QP	NS	W	Total	
	891	39	141	1,158	214	2,443	

1. W-NS-*n*, *W* wet packing, *NS* natural sand, *n* batch number; 2. binder:sand = 45%:55% by vol.; 3. (SF + QP) replaces binder by 20% by vol.; 4. SF:QP = 25%:75% by vol.; 5. W/B = 0.20; 6. SP and DF amount is 4% and 0.1% of binder, respectively

is 78.5% which is a little lower than the solid ratio of 79.3% for W-RS-3 (see Table 6).

4 UHPC/UHPFRC and Mechanical Properties

4.1 UHPC

As summarized in Table 10, 28d compressive strength of the two optimum mixes was 86.3 MPa for RS-U-20, and 90.1 MPa for NS-U-20. Additional mixing with RS was performed using lower water-to-binder ratios (W/B = 0.18, 0.17, and 0.16) as well as an additional mixing with NS (W/B = 0.16). The mix proportion of the

constituents determined by the packing density tests was kept the same for all additional mixes (see Table 8).

4.1.1 Flowability of Fresh Mixtures

The flowability of the fresh mixtures was determined by using the flow table test following KS L 5111 (2017) with results included in Table 9 and Fig. 6a, which show that the flowability of the fresh UHPC mixtures with NS and RS is similar at W/B = 0.20, and the flowability decreases consistently with decreasing W/B from 0.20 to 0.16.

Table 8 UHPC/UHPFRC mix proportions

Index	Mix design (kg/m ³)									W/B
	OPC	FA	SF	QP	RS	NS	W	SP	SSF	
NS-U-20 (W-NS-1)	891	–	39.3	141	–	1150	214	42.9	–	0.20
NS-U-16	931	–	41.0	147	–	1201	179	44.8	–	0.16
RS-U-20 (W-RS-3)	818	72.1	80.1	95.6	1084	–	199	42.6	–	0.20
RS-U-18	823	72.6	80.6	96.2	1092	–	193	42.9	–	0.18
RS-U-17	832	73.4	81.5	97.2	1104	–	184	43.4	–	0.17
RS-U-16	842	74.2	82.4	98.3	1116	–	175	43.9	–	0.16
RS-F-17-1.0	832	73.4	81.5	97.2	1104	–	184	48.8	78	0.17
RS-F-17-2.0	832	73.4	81.5	97.2	1104	–	184	48.8	156	0.17
RS-F-17-3.0	832	73.4	81.5	97.2	1104	–	184	48.8	234	0.17
RS-F-16-2.0	842	74.2	82.4	98.3	1116	–	175	49.3	156	0.16

1. RS/NS-U/F-xx-y: RS/NS recycled sand/natural sand, U/F UHPC/UHPFRC, xx W/B (%), yy SSF volume (% concrete by volume); 2. SP amount is 4.0% of binder by wt. for all UHPC mixes; 3. SP amount is 4.5% of binder by wt. for all UHPFRC mixes

Table 9 Flowability of fresh mixtures (unit: cm)

Type	UHPC						UHPFRC			
	NS-U-20	NS-U-16	RS-U-20	RS-U-18	RS-U-17	RS-U-16	RS-F-17-1.0	RS-F-17-2.0	RS-F-17-3.0	RS-F-16-2.0
No jolting	23.9	11.4	24.9	16.9	14.1	14.0	13.1	13.8	11.5	10.5
Jolting	25.4	13.6	25.4	22.1	18.6	16.8	18.5	18.0	16.0	13.7

Jolting—fresh mortar placed on the flow table was vertically shook 25 times following KS L 5111

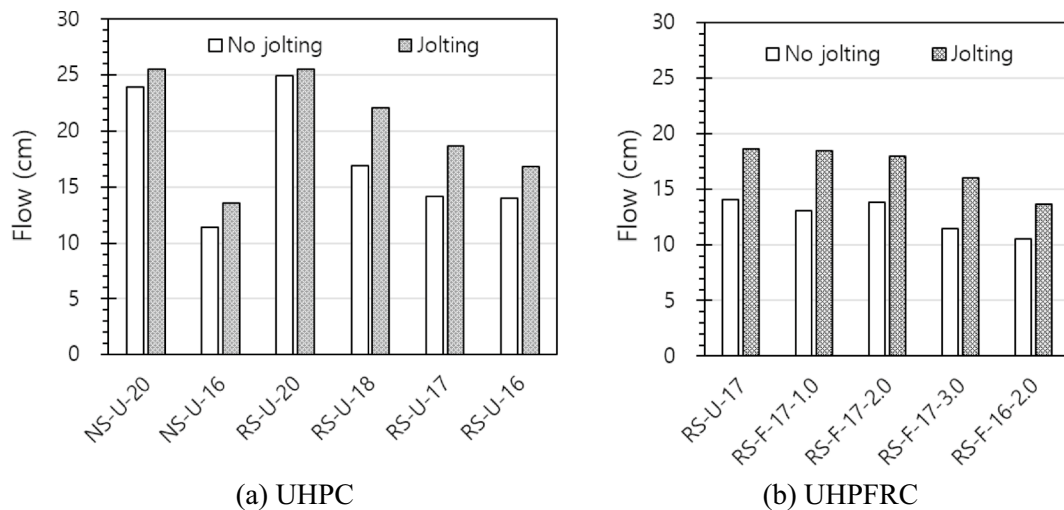


Fig. 6 Flow of fresh mixture

4.1.2 Voids, Absorption and Density of Hardened Concretes

The pore volume (voids) of the hardened concretes was determined using ASTM C642 (2013), which is known to provide a consistent measure of the pores in the paste matrix of concrete (Bu, 2014). Fig. 7a shows that the voids of NS-U-20 and RS-U-20 are similar and that

the voids of concretes with W/B=0.20 and 0.18 (RS-U-20, RS-U-18), are greater than 10% while they are about 9% or less for concretes with W/B=0.17 and 0.16 (9.3%, 8.8%, 6.4% for RS-U-17, RS-U-16, NS-U-16, respectively). The water absorption decreases with decreasing W/B and is 5.92%, 4.90%, 4.52% and 4.24% for RS-U-20, RS-U-18, RS-U-17, and RS-U-16, respectively, while it

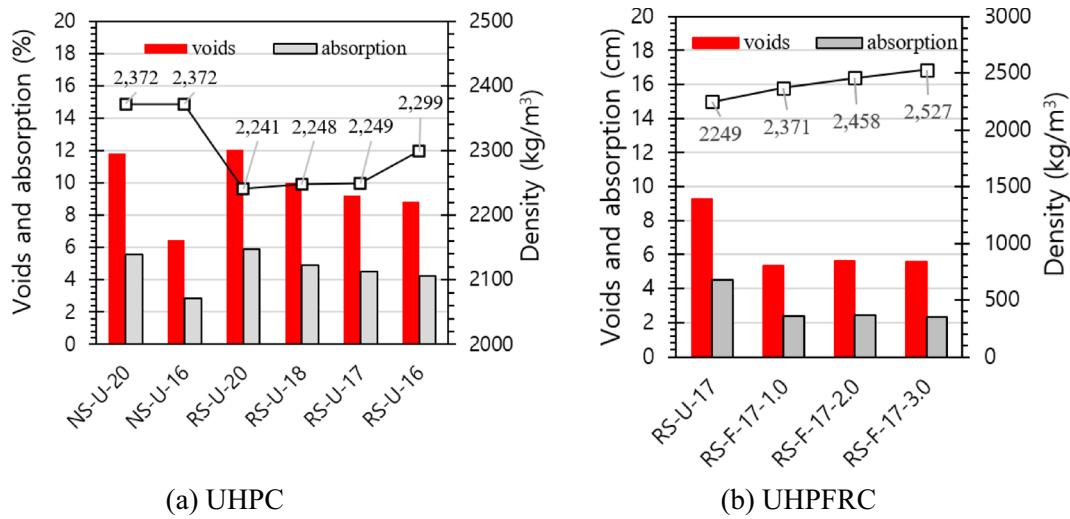


Fig. 7 Voids, water absorption and apparent density of hardened concrete

Table 10 Summary of compressive strength development, flexural strength and elastic modulus (unit: MPa)

Index	Compressive strength			Flexural strength	Index	Compressive strength			Flexural strength
	7d	28d	Elastic modulus			7d	28d	Elastic modulus	
NS-U-20	60.2	90.1	43,773	11.1	NS-U-16	63.7	112	48,043	13.5
RS-U-20	64.4	86.3	37,355	8.38	RS-F-17-1.0	75.6	100	43,506	9.41
RS-U-18	65.0	87.4	35,544	10.6	RS-F-17-2.0	84.5	128	46,867	11.9
RS-U-17	65.5	102	40,153	11.0	RS-F-17-3.0	84.5	113	46,645	18.1
RS-U-16	60.7	97.4	41,231	8.12	RS-F-16-2.0	89.6	108	47,502	14.0

is 2.86% for NS-U-16. Apparent density was also determined following ASTM C642 procedure as shown in Fig. 7a. The density of RS-U-20 (2241 kg/m³) is 94.5% of the density of NS-U-20 (2372 kg/m³) as the density of NS is higher than that of RS (see Table 2). The apparent density of UHPCs with RS tends to increase with decreasing water-to-binder ratio (i.e., with increasing solid content) as shown in Fig. 7a.

4.1.3 Compressive Strength

The development of compressive strength of concretes is summarized in Table 10 and Fig. 8. Both 7d compressive strength (64.4 MPa) and 28d compressive strength (86.3 MPa) of RS-U-20 are comparable those of the reference mix, NS-U-20 (60.2 MPa at 7d, 90.1 MPa at 28d), in Table 10 and Fig. 8a. The 28d compressive strength of concretes with RS increases in general with decreasing water-to-binder ratio as shown in Fig. 8a. In Table 10,

the 28d strength increases from 86.3 MPa for RS-U-20 to 102 MPa for RS-U-17, but the 28d strength of RS-U-16 (97.4 MPa) is a little lower than that of RS-U-17. It should be noted that, in the current study, the optimum packing density design including water was experimentally determined only for the mixture with W/B=0.20 (RS-U-20, see Clause 3.2). Test results indicate that there was not sufficient amount of water to lubricate solid particles for RS-U-16.

4.1.4 Flexural Strength and f_t/f_c

The flexural strength (f_t) was tested 28d after casting. In Table 10 and Fig. 9a, the flexural strength of concretes with NS (11.1–13.5 MPa) is higher than that of concretes with RS (8.4–11.0 MPa) and the ratio of the flexural strength to the 28d compressive strength (f_t/f_c) is 12.1–12.3% and 8.3–12.2%, for concretes with NS and with RS, respectively.

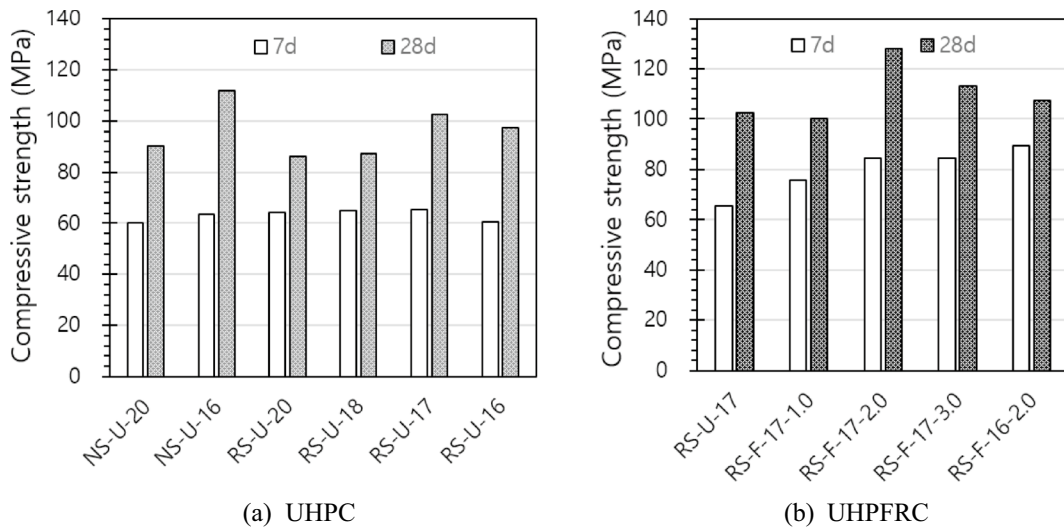


Fig. 8 Compressive strength development

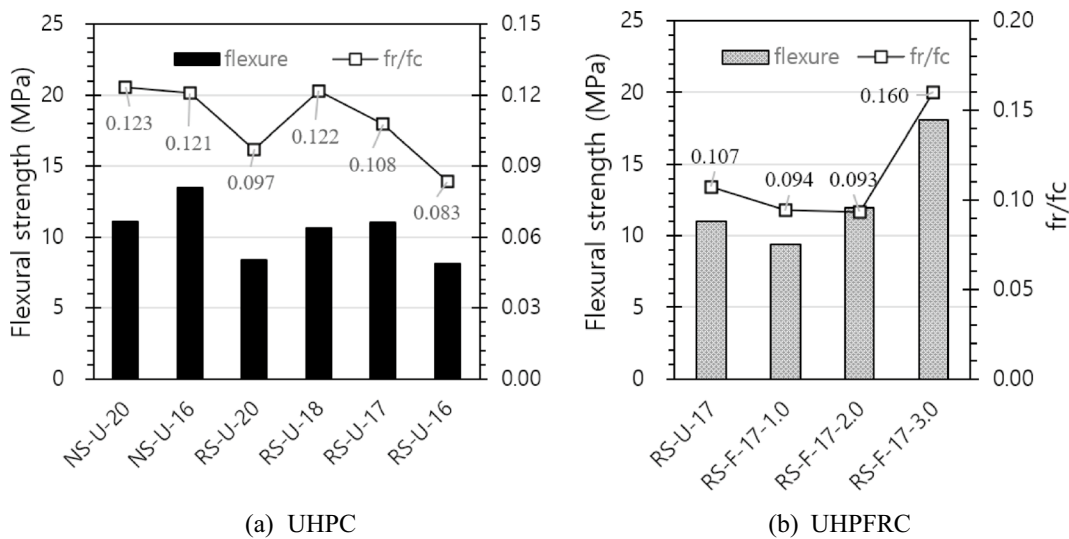


Fig. 9 Flexural strength and flexural strength-to-compressive strength ratio (f_r/f_c)

4.2 UHPFRC

Table 8 also shows the mix proportions of three UHPFRCs based on UHPC mix of RS-U-17 and SSF contents of 1%, 2%, or 3% (RS-F-17-1.0, RS-F-17-2.0, RS-F-17-3.0) by volume of concrete, as well as an additional UHPFRC mix based on RS-U-16 with SSF contents of 2.0% (RS-F-16-2.0). The flowability of the fresh mixtures with $W/B=0.17$ is not significantly affected with addition of 1% and 2% SSFs as shown in Table 9 and Fig. 6b, although the flowability significantly decreases with inclusion of 3% SSFs.

In Fig. 7b, the voids of all UHPFRCs (RS-F-17-1.0, RS-F-17-2.0, RS-F-17-3.0) with 1.0%, 2.0%, 3.0% SSFs

are 5.4%-5.7% as determined by ASTM C642 procedure. The water absorption of all UHPFRCs ranges between 2.3 and 2.45% while it is 4.5% for RS-U-17. The density ranges between 2249 and 2527 kg/m^3 and is consistently increasing with increasing amount of SSFs as the density of RS-F-17-1.0, RS-F-17-2.0, and RS-F-16-3.0 is 5.4%, 9.3%, and 12.4% higher than that of RS-U-17, respectively. In Table 10, 28d compressive strength of RS-F-17-1.0 with $W/B=0.17$ and SSF content of 1.0% (100 MPa) is similar to that of RS-U-17 at the same $W/B=0.17$ without any fibers (102 MPa). With increasing amount of fibers, the 28d strength of 128 MPa is reached at $W/B=0.17$ and with SSF content of 2.0% (RS-F-17-2.0). However,

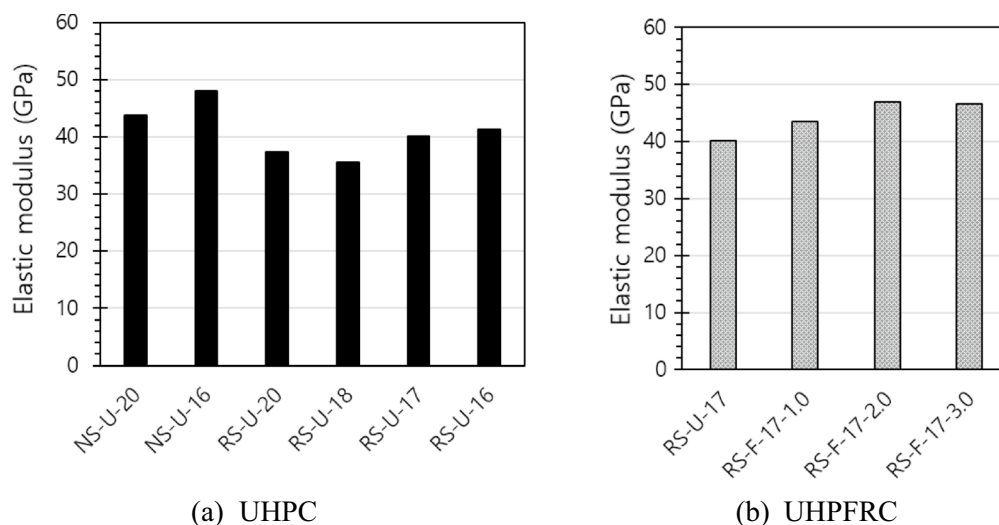


Fig. 10 Elastic modulus

the compressive strength of the UHPC at $W/B=0.17$ and with SSF content of 3.0% (RS-F-17-3.0) decreases to 113 MPa as shown in Table 10 and Fig. 8b. The flexural strength of UHPFRCs with 1.0% (RS-F-17-1.0), 2.0% (RS-F-17-2.0), and 3.0% (RS-F-17-3.0) SSFs (9.4 MPa, 11.9 MPa, 18.1 MPa) decreases by 14%, increases by 8%, and significantly increases by 65%, respectively, from that of RS-U-17 (11.0 MPa) without any fibers as shown in Table 10 and Fig. 9b. The flexural strength-to-28d compressive strength ratio (f_r/f_c) is 0.094–0.16 for UHPFRCs with SSF contents of 1–3% (RS-F-17-1.0, RS-F-17-2.0, RS-F-17-3.0).

4.3 Elastic Modulus and Poisson's Ratio

4.3.1 Elastic Modulus

$\Phi 100$ mm \times 200 mm cylinders were used to monitor the stress–strain relationship under uniaxial compression. Readings from the compressometer equipped with a pair of LVDTs (50-mm gauge length) were used to determine the stress-vs-strain relationship under uniaxial compression, while two pairs of 60-mm strain gauges per cylinder (a pair of strain gauges was installed in the vertical direction and the other pair was installed in the horizontal direction at cylinder mid-height) were used to determine the elastic modulus and the Poisson's ratio following ASTM C469 (2022) procedure. Two replicate cylinders were tested.

The elastic modulus of two concretes with NS (NS-U-20 and NS-U-16) is 43.8 GPa and 48.0 GPa, respectively, while that of two concretes with RS (RS-U-20 and RS-U-16) is 37.4 GPa and 41.2 GPa, respectively, in Table 10. The elastic modulus of UHPCs with NS is about 17% greater than that of UHPCs with RS at

the same water-to-binder ratio ($W/B=0.20$ or 0.16) as shown in Table 10 and Fig. 10a. The reduced stiffnesses determined for concretes with RS are due to use of the recycled sand. As the adhered mortar in RS introduces thicker and softer interfacial transition zones (ITZs), the elastic modulus of concretes with RS is lower than that of concretes with NS (Chinzorigt et al., 2020; Li et al., 2012). In Table 10 and Fig. 10b, the elastic modulus increases with the use of SSFs and it is 43.5 GPa, 46.9 GPa, and 46.6 GPa for RS-F-17-1.0, RS-F-17-2.0, and RS-F-17-3.0, respectively, which corresponds to 8.2%, 16.7%, and 15.9% increase over that of RS-U-17 without any fibers (40.2 GPa). Overall, the stiffness of the UHPCs with NS is 43.8–48.0 GPa, the stiffness of the UHPCs with RS is 35.5–41.2 GPa, and it is 43.5–47.5 GPa for the UHPFRCs with RS.

4.3.2 Poisson's Ratio

The stress- vs.-strain plots obtained by testing $\Phi 100$ mm \times 200 mm cylinders under uniaxial compression are shown in Fig. 11 and the Poisson's ratio determined by ASTM C469-22 procedure is summarized in Table 11 for four UHPCs with RS (RS-U-16, RS-U-20) and NS (NS-U-16, NS-U-20) as well as three UHPFRCs with RS and 1.0%, 2.0%, and 3.0% SSFs (RS-F-17-1.0, RS-F-17-2.0, RS-F-17-3.0). In Table 11, the Poisson's ratio of RS-U-20 and RS-U-16 is 0.187 and 0.199 while it is 0.215 and 0.216 for NS-U-20 and NS-U-16, respectively. While current test results seem to indicate that the Poisson's ratio of UHPCs with RS may decrease a little from that of UHPCs with NS, this observation should be further investigated in the future due to limited number of test data (2 replicate specimens).

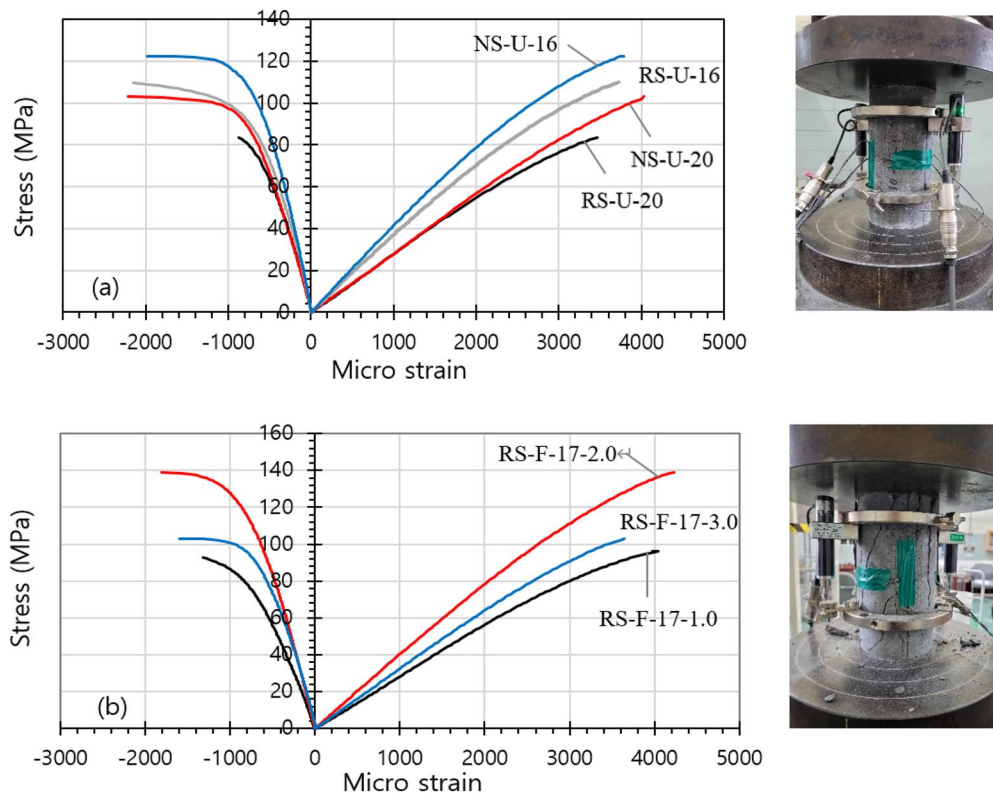


Fig. 11 Stress versus strain: uniaxial compression: **a** UHPC, **b** UHPFRC

Table 11 Poisson's ratio

Index	RS-U-20	RS-U-16	NS-U-20	NS-U-16	RS-F-17-1.0	RS-F-17-2.0	RS-F-17-3.0
Poisson's ratio	0.187	0.199	0.215	0.216	0.215	0.216	0.197

4.4 Autogenous Shrinkage

The results of the autogenous shrinkage strain measurement for 84 days after initial set for three different concretes, NS-U-20, RS-U-20, RS-U-17, with water-to-binder ratio of 0.20, 0.20, and 0.17, respectively, are shown in Fig. 12. Fig. 12 shows that the evolution of the autogenous shrinkage of NS-U-20 is very fast in the beginning and fast for about 7 days, and the shrinkage development slows down as it steadily increases with time after 7 days. For RS-U-20, the early-age autogenous shrinkage development is again fast at early ages and then increases more slowly. It can be observed that the slope of the autogenous shrinkage-vs-time curves of both NS-U-20 and RS-U-20 is about the same after 4 weeks. The autogenous shrinkage of RS-U-17 is larger than that of RS-U-20 due to reduced W/B ratio. 84 days after casting, the maximum autogenous shrinkage is 1 027 $\mu\text{m}/\text{m}$, 677 $\mu\text{m}/\text{m}$, and 857 $\mu\text{m}/\text{m}$, respectively, for NS-U-20, RS-U-20, and RS-U-17. The measured

autogenous shrinkage after 84 days is largest for NS-U-20 while it is 65.9% (about 2/3) of that for RS-U-20 at the same water-to-binder ratio ($W/B=0.20$). The autogenous shrinkage is smaller for RS-U-20 because RS provided in SSD condition provides the internal curing effect: i.e., part of water included in the porous adhered mortar of RS is used for the cement hydration which delays the self-desiccation. The autogenous shrinkage strain of RS-U-17 ($W/B=0.17$) 84 days after casting is larger than that of RS-U-20 by 26.6%, and is smaller than that of NS-U-20 by 16.6%. Current results agree with existing research results although there are few existing studies on the autogenous shrinkage of UHPC with recycled fine aggregates. Wang et al., (2021a, 2021b) reported that the autogenous shrinkage of concrete with 100% recycled coarse aggregate exhibited 46.3–65.8% smaller autogenous shrinkage for W/C ratios of 0.3–0.6 due to internal curing effect. Zhang et al. (2020) reported that both recycled fine aggregate (RFA) and recycled coarse aggregate

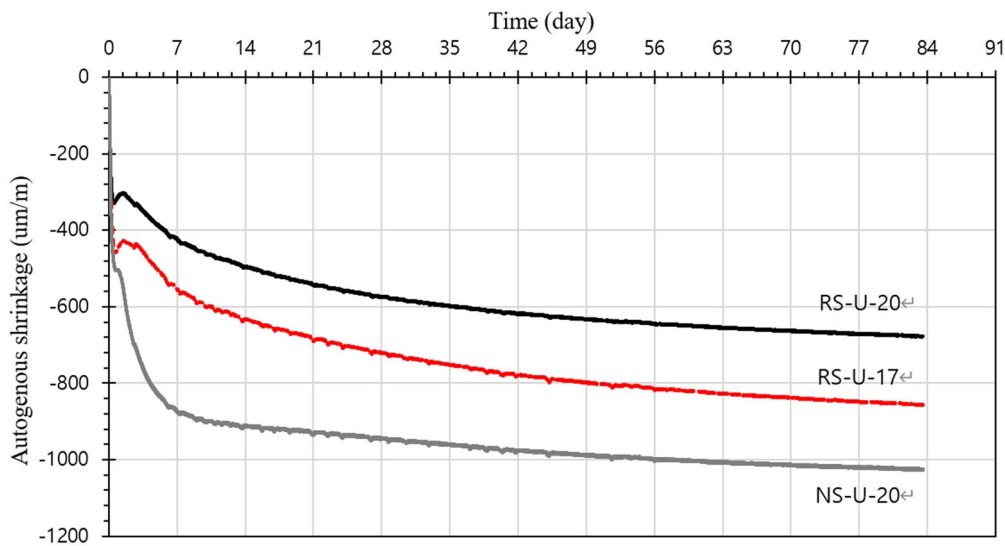


Fig. 12 Autogenous shrinkage evolution with time: UHPCs with RS and NS

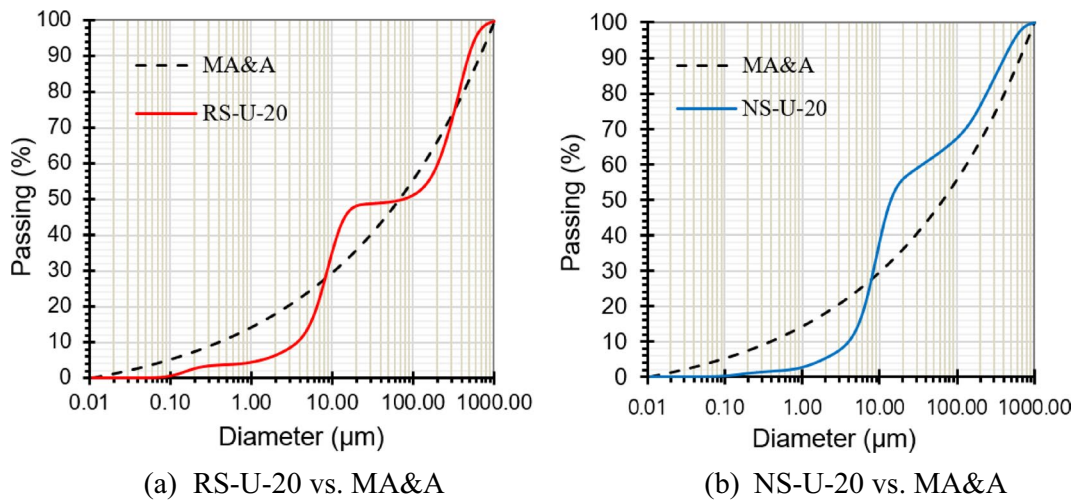


Fig. 13 Experimental packing vs. MA&A ($q=0.23$)

(RCA) significantly reduced the autogenous shrinkage of recycled aggregate concrete, and the influence of RFA is more significant with increasing content of RCA.

5 Discussion

5.1 Experimental Versus Theoretical Packing Density Approach

To determine the optimum mix proportions, an existing experimental packing density methodology proposed by Kwan and Fung (2009) was employed to develop UHPC. The optimum particle distributions determined by the experimental methodology was compared with that determined by a theoretical model, i.e., modified

Andreasen & Andersen model (MA&A), which is one of the well-known theoretical models along with LPDM (Yu et al., 2015). Fig. 13 shows relatively good match between the curve suggested by MA&A and the particle distributions determined by the experimental approach for RS-U-20 and NS-U-20, while the difference between the actual particle distribution and the MA&A curve is smaller for RS-U-20 than it is for NS-U-20 (by 15% in terms of least errors). On the other hand, the results of the wet packing density tests show that the solid ratio is 79.1% for W-RS-3 (same as RS-U-20) while the solid ratio is 78.5% for W-NS-1 (same as NS-U-20) in Tables 6 and 7, indicating a little more efficient packing for RS-U-20

Table 12 Total porosity and average pore diameter of UHPC/UHFRC samples

Item	NS-U-16	RS-U-16	RS-F-17-2.0
Total porosity (%)	10.3	14.2	12.5
Average pore diameter (nm)	14.2	18.7	20.3

over NS-U-20. As RS affects the mechanical properties of UHPC by introducing more interfacial transition zones (ITZs), the hardness of ITZ decreases and the thickness of ITZ increases in concretes with RS, which negatively affects the strength and the stiffness.

5.2 Effect of Using Recycled Sand on Microstructural Properties

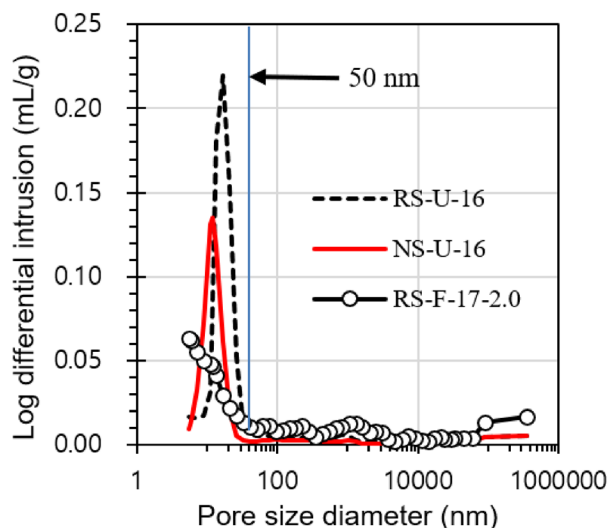
5.2.1 Porosity (MIP)

Table 12 and Fig. 14 show the results of mercury intrusion porosimetry (MIP) test of three UHPC/UHFRC samples. Total porosity is 10.3% and 14.2% after 28 days for NS-U-16 and RS-U-16, respectively, in Table 12. The average pore diameter is 14.2 nm for NS-U-16 and it is 18.7 nm for RS-U-16. The MIP test results show that, although the total porosity and the average pore diameter are small and most pores are micropores smaller than 50 nm, both the total porosity and the average pore size are larger for RS-U-16 than they are for NS-U-16 at the same water-to-binder ratio ($W/B=0.16$). This should be attributed to the fact that RS has rougher surface texture than NS, and the concrete with RS includes more porous interfacial

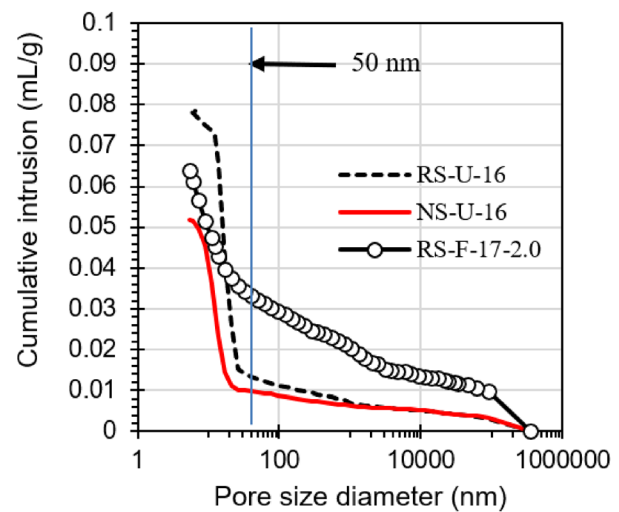
transition zones (ITZs) than the concrete with NS (Undram et al., 2022). In Table 12, the total porosity is 12.5% and the average pore diameter is 20.3 nm for the UHFRC sample with 2% SSFs and water-to-binder ratio of 0.17 (RS-F-17-2.0). While both the total porosity and the average pore size are comparable to those of two UHPC samples with water-to-binder ratio of 0.16, there are more detrimental macro pores larger than 50 nm for RS-F-17-2.0 as shown in Fig. 14b (Mehta & Monteiro, 1993). Hannawi et al. (2016) claimed that the steel fibers have compact fiber/matrix interfacial zone compared to synthetic fibers. Results shown in Fig. 14b and Table 12 indicate that the introduction of the fibers can induce macro pores between the fibers as well as between the fibers and the matrix.

5.2.2 SEM

Scanning electron microscope (SEM) images of UHPCs were taken using Hidachi SV3500 with results shown in Fig. 15. Magnified SEM images are shown in Fig. 15a, c and e for RS-U-20, RS-U-17, and NS-U-20, respectively. Fig. 15b, d and f also shows the high-resolution images of back scattered electron SEM (SEM-BSE) which also indicates the spot of the sample where the more magnified images were taken. Fig. 15a shows that the interfacial zone between RS and the cement matrix is a combination of partly dense region and the cracked region although the cement matrix is relatively free of cracks and dense with cement hydration products for RS-U-20. In Fig. 15c, good bonding and dense ITZ can be identified while cracks also exist along the interfacial zone between RS

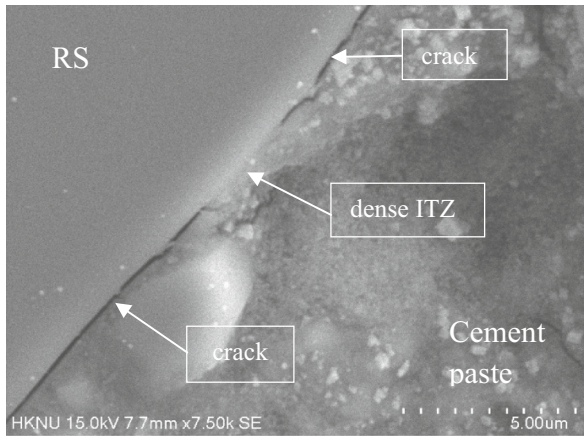


(a) Log differential intrusion

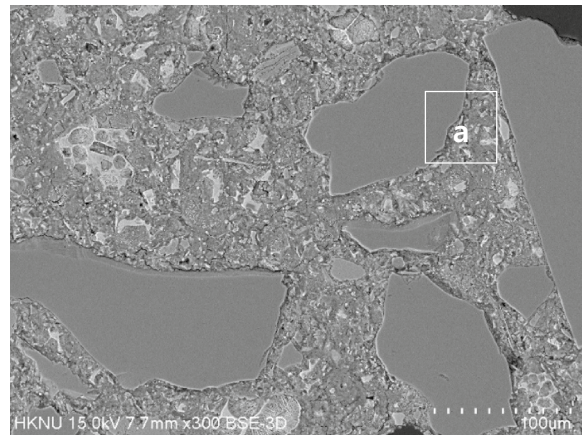


(b) Cumulative intrusion

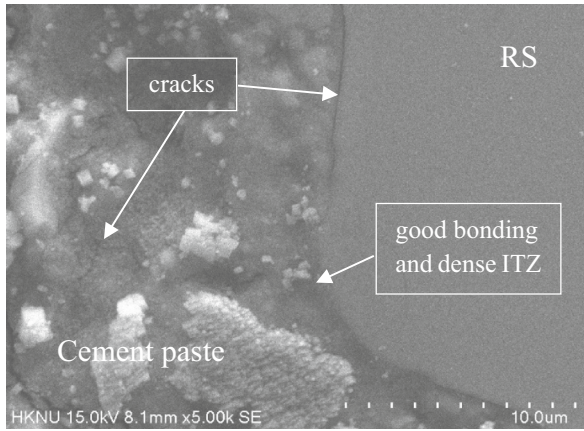
Fig. 14 Pore size distribution by MIP: NS-U-16, RS-U-16, RS-F-17-2.0



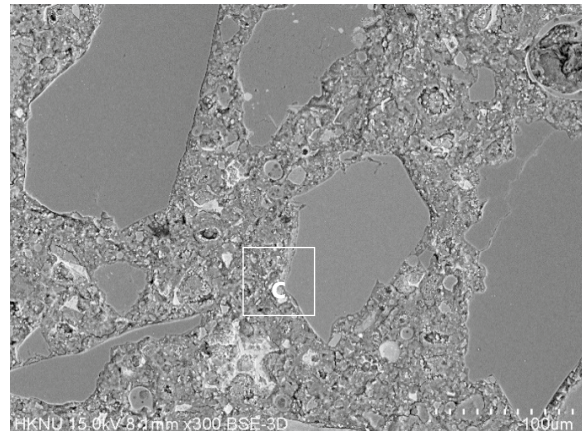
(a) SEM: RS-U-20



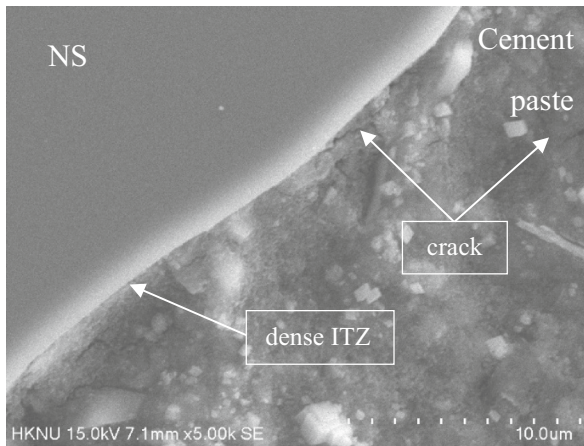
(b) SEM-BSE: RS-U-20



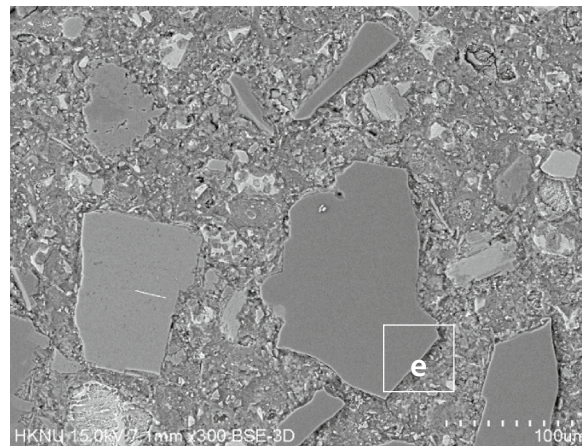
(c) SEM: RS-U-17



(d) SEM-BSE: RS-U-17



(e) SEM: NS-U-20



(f) SEM-BSE: NS-U-20

Fig. 15 SEM images of UHPCs

Table 13 LCI data used in life cycle assessment

Input material	Database name	Published year	Source
OPC	Cement, Portland (ROW), Cut-off	2018	SimaPro 9.0
Silica fume	Silica fume, densified (GLO), Cut-off	2018	SimaPro 9.0
Quartz powder	Limestone, Crushed for mill (CH), Cut-off	2018	SimaPro 9.0
Water	Tap water(ROW), Cut-off	2018	SimaPro 9.0
Natural sand	Sand(GLO), Cut-off	2018	SimaPro 9.0
Recycled sand	Recycled sand	2022	Kim and Jang (2022)

RoW rest of world, GLO global; CH—Swiss

and the cement matrix and in the cement matrix for RS-U-17. Fig. 15e shows good bonding between NS and the cement matrix for NS-U-20, although some cracks are seen near the interface and in the cement matrix.

5.3 Environmental Impacts and Economical Aspects

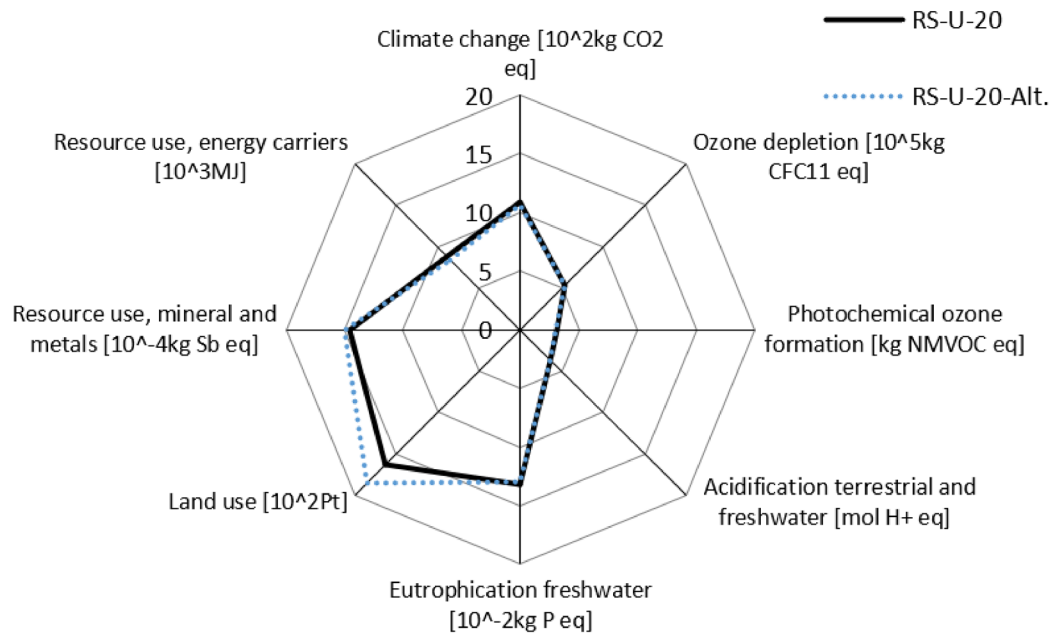
All concretes in this work used recycled sand, RS, except for two reference concretes which used natural crushed sand, NS, in an effort to save on the consumption of natural resources. At the same time, relatively low amount of OPC (818–842 kg/m³) was used for the mixes with RS while the OPC amount was a little higher for the reference mixes with NS (891–931 kg/m³). The environmental impacts of concretes with RS and NS, were compared through life cycle assessment (LCA) following ISO 14040 (2006) procedure. The following impact categories were selected to summarize the results of the LCA study as suggested by ISO 13315–8 (2019): Global climate change, stratospheric ozone level, acidification, eutrophication, photochemical ozone creation, natural resources use (fuel and resources), as well as land use. Built-in LCI data of SimaPro version 9.0 were used while the LCI data for RS were provided by Kim and Jang (2022) as shown in Table 13. The system boundary was cradle-to-gate. Transportation distance for RS and NS was set to be the same (200 km) and the method of transportation was by trucking. Fig. 16 shows the results of two different sets of LCA studies: (1) first set—comparison between RS-U-20 vs. NS-U-20; (2) second set—comparison between RS-U-20 vs. RS-U-20-Alt. The first comparison was made between two different mix designs of RS-U-20 and NS-U-20. The second comparison was necessary as the mix designs of RS-U-20 and NS-U-20 are not the same, although they resulted in similar strength development (see Table 10 and Fig. 8a). In the second comparison by the LCA study, the same mix design was used for both mixes (RS-U-20 and RS-U-20-Alt.) where RS-U-20 used RS and RS-U-20-Alt. used NS. In Fig. 16a, the area of octagon is smaller for RS-U-20 than that of NS-U-20. Therefore, RS-U-20 has smaller environmental impact in overall than NS-U-20. The environmental impact of RS-U-20 in the impact category of climate change, ozone

depletion, photochemical ozone formation, acidification, eutrophication, land use, non-biotic resource use is smaller by 6%, 7%, 1%, 3%, 4%, 21%, and 7%, respectively, than that of NS-U-20. RS-U-20 has advantages over NS-U-20 especially for land use and non-biotic resource depletion. It should be noted that the climate change is more for NS-U-20 as the mix design of this concrete uses a little larger amount of OPC than RS-U-20 (see Table 8). In Fig. 16b, the area of octagon for RS-U-20 is again smaller than that of NS-U-20 indicating the reduced environmental impact of RS-U-20 from that of RS-U-20-Alt. Impact from ozone depletion, land use, and non-biotic resource use is 2%, 14%, and 3% smaller for RS-U-20 than it is for RS-U-20-Alt. On the other hand, climate change, ozone formation, acidification, eutrophication, and biotic resource use are 2%, 4%, 3%, 2%, and 4% greater for RS-U-20 than it is for RS-U-20-Alt. It is noted that the climate change is 2% larger for RS-U-20 than RS-U-20-Alt. probably due to extensive crushing procedure needed to produce high-quality RS, as shown in Fig. 2 (JSCE-7, 2006).

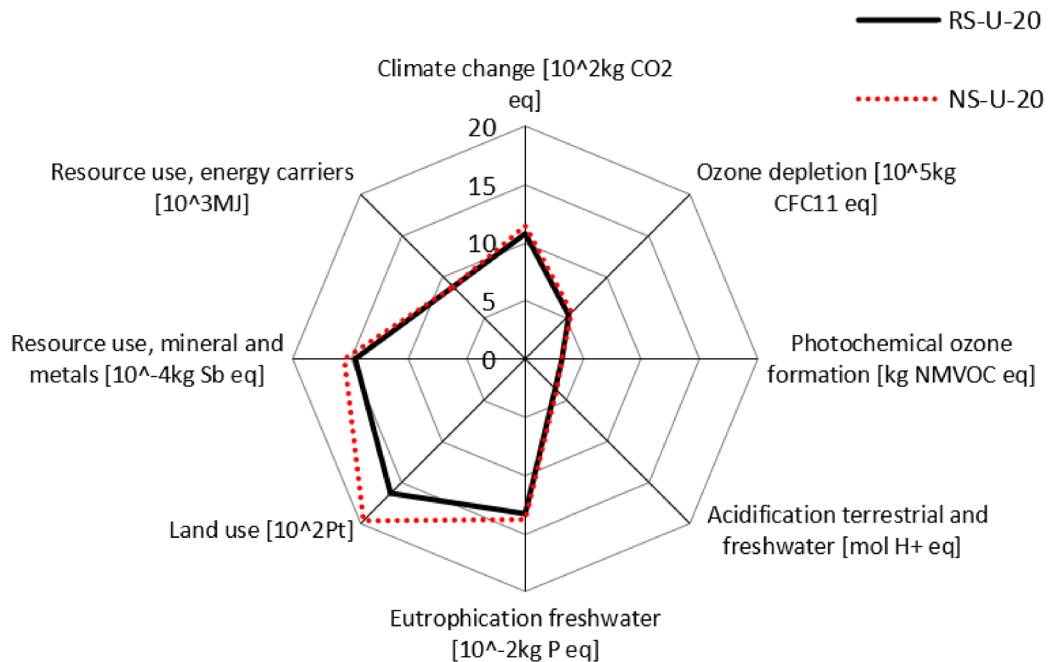
Fig. 17 shows the cost comparison between RS-U-20 and NS-U-20 per unit strength and per unit volume of concrete. Fig. 17 includes OPC, SCMs, filler and sand only (the chemical admixture SP, although it takes significant portion of total cost, is not shown because both RS-U-20 and NS-U-20 used the same amount). The total cost of NS-U-20 is about 9% higher than that of RS-U-20 per unit volume. The cost implication of using RS is not large as two dominant components are OPC and QP. Fig. 17 suggests that, to lower the total production cost of UHPC, it is needed to use smaller amount of OPC and replace QP with less expensive filler (such as limestone powder or other more economical filler).

6 Conclusions

The optimum mix design of UHPC with recycled sand (RS) was first determined using two-step packing density test. Based on the mix design of the UHPCs, the UHP-FRCs with recycled sand and 1–3% straight steel fibers



(a) RS-U-20 vs. NS-U-20



(b) RS-U-20 vs. RS-U-20-Alt.

Fig. 16 Environmental impacts of UHPCs with RS vs. NS

were developed. All UHPCs/UHPFRCs used 100% RS and relatively low amount of OPC (818–842 kg/m³). The following conclusions are drawn from current work:

- (1) The 28d compressive strength of the UHPC with RS was 102 MPa and the flexural strength was 11.0 MPa (W/B=0.17). With adoption of 2% brass coated straight steel fibers, the 28d strength of

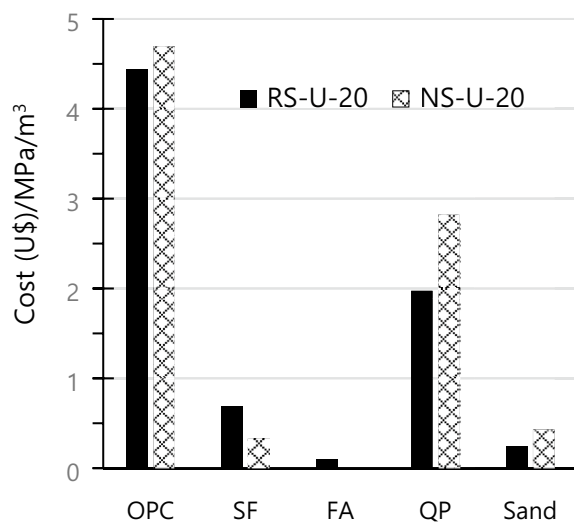


Fig. 17 Cost per unit strength: RS-U-20 and NS-U-20

the UHPFRC with RS was 128 MPa and flexural strength was 11.9 MPa.

- (2) The elastic modulus was 37.4 GPa–41.2 GPa for the UHPCs with RS ($W/B=0.16-0.20$), while that of the UHPFRCs with RS was 43.5 GPa–47.5 GPa. The elastic modulus of UHPC/UHPFRC with RS decreased from that of the reference concretes with natural crushed sand (NS) by 17%.
- (3) Autogenous shrinkage of UHPCs with RS at early ages was significantly smaller than that of the reference concrete with NS, which should be attributed to the internal curing effect provided by RS which delayed self-desiccation.
- (4) The pore structure of the UHPC with RS investigated by MIP test showed that most voids were micro pores under 30 nm for both concretes with RS and NS. However, the total porosity and the average pore diameter of the concretes with RS were 32%–38% larger than those of the concrete with NS.
- (5) The environmental impact of using RS versus NS was investigated by life cycle assessment (LCA) study. The overall environmental impact of the UHPC with RS was smaller than that of the UHPC with NS. The main advantages of using RS were land use and abiotic resource depletion. Climate change (i.e., CO_2 emission) was sensitive to scenarios, and the difference was small for the two different comparisons between the concretes with RS and that with NS in the LCA study. Economical aspects of using RS were also explored. The results indicated that the cost implication associated with the use of RS was relatively small, while the dominating components were OPC and quartz powder.

Acknowledgements

Authors appreciate generous support for this research by the National Research Foundation of Korea (NRF) funded by the Ministry of Science and ICT. (No. 2021K1A3A1A200017221112582071420101) and Construction Engineering Research Institute of Hankyong National University.

Author contributions

DC: overall research plan and control. KH: implementation of experiments. MO: implementation of experiments. DM: theoretical packing density and implementation of experiments. PS: application of experimental packing density methodology and research plan.

Funding

National Research Foundation (NRF), Republic of Korea.

Availability of data and materials

Available upon request.

Declarations

Competing interests

Not applicable.

Received: 8 April 2023 Accepted: 8 August 2023

Published online: 19 December 2023

References

- Ahmed, T., Elchalakani, M., Karrech, E., Dong, M., Mohamed Ali, M. S., & Yang, H. (2021). ECO-UHPC with high-volume class-F fly ash: New insight into mechanical and durability properties. *ASCE Journal of Materials in Civil Engineering*, 33(7), 04021174.
- Amran, M., Huang, S.-S., Onaizi, A. M., Makul, N., Abdelgader, H. S., & Ozbakaloglu, T. (2022). Recent trends in ultra-high performance concrete (UHPC): Current status, challenges, and future prospects. *Construction and Building Materials*, 352, 129029.
- ASTM C642. (2013). Standard test method for density, absorption and voids in hardened concrete, American Society for Testing and Materials, West Conshohocken, PA.
- ASTM C469. (2022). Standard test method for static modulus of elasticity and Poisson's ratio of concrete in compression, American Society for Testing and Materials, West Conshohocken, PA.
- Bahmani, H., & Mostofinejad, D. (2022). Microstructure of ultra-high-performance concrete (UHPC) – a review study. *Journal of Building Engineering*, 50, 104118.
- BS EN 206:2013+A2. (2021). Concrete—specification, performance, production and conformity, BSI
- Bu Y., Spragg R., Weiss W. (2014). Comparison of the Pore Volume in Concrete as Determined Using ASTM C642 and Vacuum Saturation. *ASTM Journal*, 3(1), 308–315.
- Chinzorig, G., Lim, M. K., Yu, M., Lee, H., Enkhbold, O., & Choi, D. (2020). Strength, shrinkage and creep and durability aspects of concrete including CO_2 treated recycled fine aggregate. *Cement & Concrete Research*, 136, 106062.
- Dawood, E. T., & Abdullah, M. H. (2021). Behavior of green reactive powder mortar reinforced with steel fibers. *Journal of the Mechanical Behavior of Materials*, 30, 130–143.
- de Brito, J., & Saikia, N. (2013). *Recycled aggregate in concrete*. Springer-Verlag.
- de Larrard, F., & Sedran, T. (1994). Optimization of ultra-high-performance concrete by the use of a packing model. *Cement and Concrete Research*, 24(6), 997–1009.
- de Larrard, F., & Sedran, T. (2002). Mixture proportioning of high-performance concrete. *Cement and Concrete Research*, 32, 1699–1704.
- Du, J., Meng, W., Khayat, K. H., Bao, Y., Guo, P., Lyu, Z., Abu-odeidah, A., Nassif, H., & Wang, H. (2021). New development of ultra-high performance concrete (UHPC). *Composites, Part B: Engineering*, 224, 109220.
- Funk, J. E., & Dinger, D. R. (1994). *predictive process control of crowded particulate suspensions: Applied to ceramic manufacturing*. Springer Science.

- Ha, N. S., Marundrury, S. S., Pham, T. M., Pournasiri, E., Shi, F., & Hao, H. (2022). Effect of grounded blast furnace slag and rice husk ash on performance of ultra-high performance concrete (UHPC) subjected to impact loading. *Construction and Building Materials*, *329*, 127213.
- Hannawi, K., Bian, H., Orince-Agbojjan, W., & Raghavan, B. (2016). Effect of different types of fibers on the microstructure and the mechanical behavior of ultra-high performance fiber-reinforced concretes. *Composites, Part B: Engineering*, *86*, 214–220.
- ISO 14040. (2006) Environmental management—life cycle assessment—principles and framework, Geneva, Switzerland.
- ISO 13315–8. (2019). Environmental management of concrete and concrete structures – Part 8: Environmental labels and declarations, Geneva, Switzerland.
- Jaramillo-Murcia, D. C., Abellan-Garcia, J., Torres-Castellanos, N., & Garcia-Castano, E. (2022). Properties analysis of ultra-high-performance concrete with recycled glass and limestone powders. *ACI Materials Journal*, *119*(5), 153–163.
- Jiang, J., Zhou, W., Gao, Y., Wang, L., Wang, F., Chu, H., Xu, G., Vandevyvere, B., Sierens, Z., & Li, J. (2019). Feasibility of manufacturing ultra-high performance cement-based composites (UHPCs) with recycled sand: A preliminary study. *Waste Management*, *83*, 104–112.
- JSCE guidelines for concrete no. 7. (2006). Recommendation of environmental performance verification for concrete structures (Draft), Japan Society of Civil Engineers
- Kim, I., & Jang, Y. (2022). Material efficiency and greenhouse gas reduction effect of industrial waste by material circulation in Korea. *Journal of Cleaner Production*, *376*, 134053.
- KS F 2573. (2014). Recycled aggregates for concrete, KATS, Republic of Korea (in Korean)
- KS L 5111. (2017). Flow table for use in tests of hydraulic cement, KATS, Republic of Korea (in Korean).
- KS F 2586. (2021). Standard test method for autogenous shrinkage and expansion of cement, paste, mortar and concrete, KATS, Republic of Korea (in Korean)
- Kwan, A. K. H., & Fung, W. W. S. (2009). Packing density measurement and modeling of fine aggregate and mortar. *Cement & Concrete Composites*, *31*, 349–357.
- Leng, Y., Lui, Y., Zhonghe, S., Dingqiang, F., Jinnan, W., Yonghuan, Y., Qiqing, L., & Xiang, H. (2023). Development of an environmental Ultra-High Performance Concrete (UHPC) incorporating carbonated recycled coarse aggregate. *Construction and Building Materials*, *362*, 129657.
- Li, W., Xiao, J., Sun, Z., Kawashima, S., & Shah, S. (2012). Interfacial transition zones in recycled aggregate concrete with different mixing approaches. *Construction and Building Materials*, *35*, 1045–1055.
- Luo, B., Deng, C., & Luo, Y. (2022). Mechanical properties and microstructure of UHPC with recycled glasses after exposure to elevated temperatures. *Journal of Building Engineering*, *62*, 105369.
- Mao, X., Qu, W., & Zhu, P. (2019). Mixture optimization of green reactive powder concrete with recycled powder. *ASCE J. of Materials Division*, *31*(5), 04019033–04019041.
- Mehta, P. K., & Monteiro, J. M. (1993). *Concrete* (2nd ed.). Prentice Hall.
- Naidanjav, U., Ochirbud, M., & Choi, D. (2022). Development of 100-MPa green reactive powder concrete using 100% recycled aggregates. *Journal of Asian Concrete Federation*, *8*(2), 9–22.
- Ravichandran, D., Prem, P. R., & Kaliyavaradhan, S. K. (2022). Influence of fibers on fresh and hardened properties of Ultra High Performance Concrete (UHPC)—A review. *Journal of Building Engineering*, *57*, 104922.
- Richard, P., & Cheyrezy, M. (1995). Composition of reactive powder concrete. *Cement and Concrete Research*, *25*(7), 1501–1511.
- Salahuddin, H., Qureshi, L. A., Nawaz, A., & Raza, S. S. (2020). Effect of recycled fine aggregates on performance of reactive powder concrete. *Construction and Building Materials*, *243*, 118223.
- Silva, R. V., de Brito, J., & Dhir, R. K. (2014). Properties and composition of recycled aggregates from construction and demolition wastes suitable for concrete production. *Construction and Building Materials*, *65*, 201–217.
- Sohail, M. G., Wang, B., Jain, A., Kahraman, R., Ozerkan, N. G., Gencturk, B., Eawood, M., & Belarbi, A. (2018). Advancements in concrete mix designs: high-performance and ultrahigh-performance concretes from 1970 to 2016. *ASCE Journal of Materials in Civil Engineering*, *30*(3), 04017310.
- Soliman, N. A., & Tagnit-Hamou, A. (2017). Partial substitution of silica fume with fine glass powder in UHPC: Filling the micro gap. *Construction and Building Materials*, *139*, 374–383.
- Stovall, T., Larrard, F., & Buil, M. (1986). Linear packing density model of grain mixtures. *Powder Technology*, *48*, 1–12.
- Wang, B., Yan, L., & Fu, Q. (2021a). A comprehensive review on recycled aggregate and recycled aggregate concrete, *Journal of Resources. Conservation and Recycling*, *171*, 105565.
- Wang, Q., Wang, Y.-Y., Geng, Y., & Zhang, H. (2021b). Experimental study and prediction model for autogenous shrinkage of recycled aggregate concrete with recycled coarse aggregate. *Construction and Building Materials*, *268*, 121197.
- Yang, J., Chen, B., Su, J., Xu, G., Zhang, D., & Zhou, J. (2022). Effect of fibers on the mechanical properties of UHPC: A review. *Science Direct*, *9*(3), 363–387.
- Yu, R., Spiesz, P., & Brouwers, H. J. H. (2015). Development of Ultra-High Performance Fibre Reinforced Concrete (UHPRC): Towards an efficient utilization of binders and fibres. *Construction and Building Materials*, *79*, 273–282.
- Yu, Z., Wu, L., Zhang, C., & Bangi, T. (2023). Influence of eco-friendly finer aggregate on macroscopic properties, microstructure and durability of ultra-high performance concrete: A review. *Journal of Building Engineering*, *65*, 105783.
- Zhang, B., Ma, T. J. Y., & Hu, Y. (2022). Workability and strength of ultra-high-performance concrete containing Nano-Ca(OH)₂-Modified recycled fine aggregate. *ACI Materials Journal*, *119*(5), 165–174.
- Zhang, H., Ji, T., Zeng, X., Yang, Z., Lin, X., & Liang, Y. (2018). Mechanical behavior of ultra-high performance concrete (UHPC) using recycled fine aggregate cured under different conditions and the mechanism based on integrated microstructural parameters. *Construction and Building Materials*, *192*, 489–507.
- Zhang, H., Wang, Y.-Y., Lehman, D. E., & Geng, Y. (2020). Autogenous-shrinkage model for concrete with coarse and fine recycled aggregate. *Cement and Concrete Composites*, *111*, 103600.
- Zhou, Y., Guo, D., Xing, F., & Guo, M. (2021). Multiscale mechanical characteristics of ultra-high performance concrete incorporating different particle size ranges of recycled fine aggregate. *Construction and Building Materials*, *307*, 12513.

Publisher's Note

Springer Nature remains neutral with regard to jurisdictional claims in published maps and institutional affiliations.

Donguk Choi Professor, Hankyong National University Industry Academic Cooperation Foundation, Anseong, Republic of Korea.

Kyungchan Hong Graduate Research Assistant, Dept. of Architectural Engineering, Hankyong National University, Anseong, Republic of Korea.

Munkhtuvshin Ochirbud Post Graduate Researcher, Hankyong National University Industry Academic Cooperation Foundation, Anseong, Republic of Korea.

Didar Meiramov Graduate Research Assistant, Dept. of Architectural Engineering, Hankyong National University, Anseong, Republic of Korea.

Piti Sukontaskuul Professor, Dept. of Civil Engineering, King Mongkut's University of Technology North Bangkok, Bangkok, Thailand.